Research Article Vol. 32, No. 6 / 11 Mar 2024 / Optics Express 9800
Optics EXPRESS

Development of a double-grating differential interferometer for plasma diagnostics

KYUNGMIN ROH,[1] HYOJEONG LEE,[1] SEONGJIN JEON,[1] KEEKON KANG,[1,2] MIN SUP HUR,[3] AND HYYONG SUK[1,*]

[1]*Department of Physics and Photon Science, Gwangju Institute of Science and Technology (GIST), Gwangju 61005, Republic of Korea*
[2]*Present address: Korea Electrotechnology Research Institute (KERI), Changwon 51543, Republic of Korea*
[3]*Department of Physics, Ulsan National Institute of Science and Technology (UNIST), Ulsan 44919, Republic of Korea*
[*]*hysuk@gist.ac.kr*

Abstract: A special differential interferometer consisting of two gratings was developed for diagnostics of plasma density. Compared with other differential interferometers, our system has an important advantage that the shear distance, shear direction, and fringe width can be adjusted *independently*, enabling easy control of the parameters. This feature allows precise tuning of the two probe beams in the interferometer for rigorous differential phase diagnosis and more accurate information of the plasma density can be obtained. The double-grating-based differential interferometer was tested for diagnostics of the laser-produced plasma which was generated by focusing a 1 TW/35 fs Ti:sapphire laser pulse in a gas jet with a 100 μm orifice diameter. It was confirmed that our differential interferometer can provide more reliable and accurate plasma density information, especially for plasmas with a high spatial gradient in density.

1. Introduction

In recent years, there has been an increasing interest in the application of high-repetition-rate (>1 kHz) lasers for laser-plasma acceleration [1–3]. In general, the peak power of high repetition rate laser systems is limited to about 1 TW or sub-TW, and they can be used for various applications such as the ultrafast electron diffraction [4,5], electron beam radiotherapy [6,7], etc. In the case of laser-plasma acceleration by high repetition rate lasers, however, the focused laser intensity is limited, so the laser beam should be focused very tightly in a gas jet, leading to a laser-produced plasma with a high gradient in density. Interferometers are widely used for plasma density diagnostics in these case. However, diagnostics of this type of plasma is quite tricky and conventional laser interferometers can give unreliable results at some locations because amplification of errors by the numerical differentiation in the Abel inversion [8] can occur. Hence, the differential interferometry [9] would be better for diagnostics of a plasma with a high gradient in density as it measures the phase shift derivative directly.

Although there are some existing differential interferometers, we developed a better scheme of a differential interferometer for plasma diagnostics in our laboratory. This interferometer consists of two transmission gratings, where the first and second gratings are separated with a certain distance. This configuration may look similar to the Moiré deflectometer [10] or the Talbot interferometer [11]. In our interferometer, however, the first grating is positioned at the image plane of the plasma, so the plasma image does not change although the first grating is rotated. This difference in configuration leads to totally different characteristics. Unlike the Moiré deflectometer and other common interferometers like the Michelson [12], Mach-Zehnder [13,14] or Nomarski [15] interferometer, the most significant distinction of our interferometer is its capability to *independently* adjust the fringe width, shear direction and shear distance. As a result, this interferometer allows fine-tuning of the phase shifts in two probe beams which forms the

#517186 https://doi.org/10.1364/OE.517186
Journal © 2024 Received 27 Dec 2023; revised 18 Feb 2024; accepted 18 Feb 2024; published 4 Mar 2024

Optics EXPRESS

interferogram, enabling rigorous implementation of the differential interferometry for diagnostics of a plasma with a high gradient in density. In this paper, the basic concept of the differential interferometry is introduced first, and then our analytical result for the characteristics of the differential interferometer is described. After that, the experimental setup and the experimental results for plasma diagnostics with the differential interferometer are shown.

2. Differential interferometry

In this section, the general concept of the differential interferometry for laser-plasma diagnostics is introduced before description of our differential interferometer. First, let $\Delta\varphi(y, z)$ be a phase shift introduced by the plasma in one probe beam. Then, assume that the two identical probe beams propagating in direction x, each including the phase shift that forms an interference pattern, are separated in the vertical direction y (perpendicular to the main laser beam propagation direction z). The phase shifts in the interferogram can give a difference $\Delta\varphi(y, z) - \Delta\varphi(y - s, z)$, where s is the shear distance in y. In the case of the conventional interferometry, the shear distance between two phase shifts is large enough so that they are completely separated. However, if the shear distance is much smaller than the size of the plasma, the two phase shifts overlap each other. Then, the following approximation can be used to obtain the partial derivative of the phase shift as

$$\frac{[\Delta\varphi(y, z) - \Delta\varphi(y - s, z)]}{s} \approx \frac{\partial[\Delta\varphi(y, z)]}{\partial y}. \tag{1}$$

As a result, the differential interferometer measures the phase shift gradient in the sheared direction, while the conventional interferometers measure the phase shift. Using the measured phase shift information, the plasma electron density can be reconstructed using the generalized Abel inversion method for non-axisymmetric density [16]. In this case, the result for plasma density is not affected even though there is a large phase shift gradient away from the gas nozzle. Unlike the conventional interferometry that obtains the derivative of the phase shift through numerical differentiation of the measured phase shift, the differential interferometry directly measures the partial derivative value as shown in Eq. (1). Here, selecting the appropriate shear distance is important. If the shear distance is too large, the accuracy decreases. If the shear distance is too small, we will have less sensitivity. As a result, there is an optimum range in shear distance.

To apply this differential interferometry for diagnostics of a laser-produced plasma, it is crucially important to align the shear vector in the vertical direction y with an adjustability of the shear distance. But it is not trivial in other type of interferometers and that is why we developed a new differential interferometer.

3. Basic idea of the new differential interferometer

The new interferometer is based on two Ronchi gratings [17]. Each of these gratings functions as a beam splitter, directing one of the two required probe beams by diffraction to form the interference pattern. The grating consists of repeating patterns of lines that block the propagation of light. The two gratings produce a unique interference pattern and the optical schematic of the double-grating differential interferometer is shown in Fig. 1. In this scheme, a collimated laser beam passes through a plasma and the plasma is imaged by a telescope consisting of two lenses L1 and L2 with focal lengths of f1 and f2. It should be noted that the first grating G1 must be positioned at the plasma image plane in our scheme, as shown in Fig. 1. Initially, the direction of the first grating (parallel direction with the grating ruler lines) is slightly tilted to an angle θ with respect to the z direction. The second grating G2 is placed at a distance D away from the first grating G1 with the fixed angle 0° with respect to the z direction. The imaging lens L3 is used to image the sheared images of the plasma onto a CCD camera. An iris diaphragm is placed in the Fourier plane of the lens L3 as a spatial filter for the first order filtering [18].

Optics EXPRESS

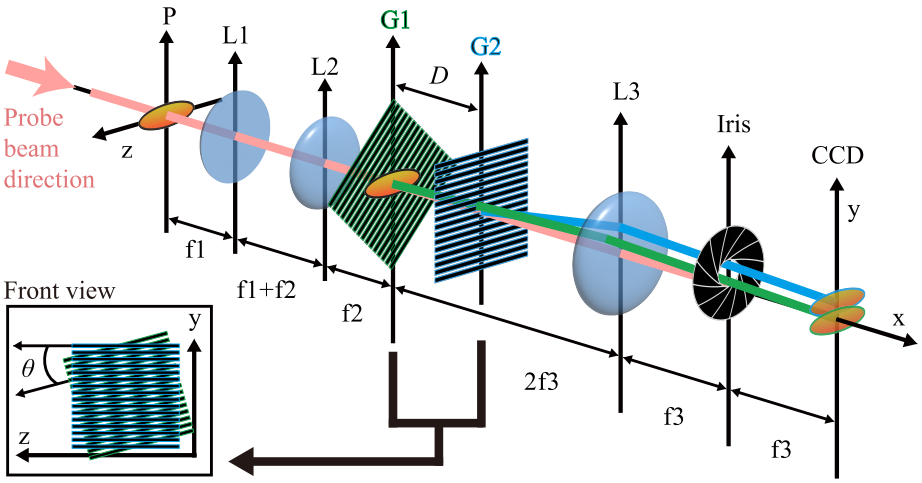

Fig. 1. Optical schematic of the novel concept of the double-grating differential interferometer. P: plasma, L: lens, G: grating, f: focal length of the corresponding lens, D: distance between the gratings. The optical components should be arranged as follows: The first grating G1 is placed in the imaged plane of the plasma and the second grating G2 is at the position distance D away from the G2. The plasma image at G1 is imaged again by the lens L3, and unnecessary high diffraction orders are filtered by the iris diaphragm that is positioned at the focal plane of the lens L3.

In this situation, the scalar diffraction theory can be used to calculate the intensity distribution on the plasma image plane imaged by the telescope. This image is the same as the intensity distribution on the CCD plane imaged by the lens L3. The electric field $E_p(y, z)$ and its Fourier transformation $U_p(y, z)$ at the position of the plasma image without the gratings can be expressed as

$$E_p(y, z) \propto \exp[ik\Delta\varphi(y, z)], \tag{2}$$

$$U_p(y, z) = F[E_p(y, z)], \tag{3}$$

where $k = 2\pi/\lambda$ is the wave vector and λ is the wavelength of the probe beam. The Fourier transformed transmission functions of the G1 and G2 are given by

$$g_1\left(\nu_y, \nu_z\right) = \sum_m a_m \delta\left(\nu_y - \frac{m}{d}\cos\theta, \nu_z + \frac{m}{d}\sin\theta\right), \tag{4}$$

$$g_2\left(\nu_y, \nu_z\right) = \sum_n a_n \delta\left(\nu_y - \frac{n}{d}, \nu_z\right), \tag{5}$$

where $\nu_y = k_y/2\pi$ and $\nu_z = k_z/2\pi$ are the transverse spatial frequencies in each direction, m and n are the diffraction orders of G1 and G2, a_m and a_n are the Fourier expansion coefficients, d is the period of the gratings, and θ is the angle of G1 relative to the z direction. Due to the separation distance D between G1 and G2, the transfer function of free space is given as

$$H\left(\nu_y, \nu_z\right) = \exp\left[ik(-D)\sqrt{1 - \lambda^2\left(\nu_y{}^2 + \nu_z{}^2\right)}\right]. \tag{6}$$

After placing the two gratings with separation distance D at the given places, the electric field $E_1(y, z)$ at the image plane can be calculated using the Fresnel approximation and the asymptotic

Optics EXPRESS

approximation. The result is given as follows:

$$\begin{aligned} E_1(y,z) =& F^{-1}\left\{\left[\left(U_p * g_1\right) H\right] * g_2\right\} \\ \approx& \exp(-ikD) \sum_{m,n} a_m a_n \exp\left(i\pi D\lambda \frac{n^2}{d^2}\right) \\ &\times \exp\left[i2\pi\left(\frac{n+m\cos\theta}{d} y - \frac{m\sin\theta}{d} z\right)\right] \exp\left[ik\Delta\varphi\left(y - \frac{D\lambda n}{d}, z\right)\right], \end{aligned} \tag{7}$$

where F^{-1} is the inverse Fourier transform and $*$ is the convolution. Other diffraction orders, except for the first order satisfying $(m = 1, n = 0)$ and $(m = 0, n = 1)$, are spatially filtered using the iris diaphragm in the focal plane of the lens L3. Consequently, the intensity of the interferogram in the image plane can be calculated as

$$\begin{aligned} I_1(y,z) =& E_1(y,z) E_1^*(y,z) \\ \propto& 1 + \cos\left\{-\frac{2\pi(1-\cos\theta)}{d} y - \frac{2\pi\sin\theta}{d} z - \frac{\pi D\lambda}{d^2}\right. \\ &\left. + k\left[\Delta\varphi(y,z) - \Delta\varphi\left(y - \frac{D\lambda}{d}, z\right)\right]\right\}. \end{aligned} \tag{8}$$

Then the shear distance s and the fringe width h can be obtained from Eq. (8):

$$s = \frac{D\lambda}{d}, \tag{9}$$

$$h = d\sqrt{\frac{2}{\sin^2\theta(1-\cos\theta)}}. \tag{10}$$

Unlike other widely-used interferometers, the most remarkable aspect of this interferometer is its capability to independently adjust the shear distance, shear direction, and fringe width, as shown in Eqs. (9) and (10). For the given probe beam and gratings, the shear distance is only dependent on the distance D and the fringe width is only dependent on the angle θ of the first grating. In addition, the shear direction is fixed in the y direction in this configuration. As a result, the two images can be precisely sheared in vertical direction with the controllable shear distance, which can realize practical applications of the differential interferometer. This is possible by positioning the first grating in the plasma image plane. Otherwise, the shear distance, shear direction and fringe width will be correlated like in other double-grating based interferometers (e.g., Moiré deflectometer or Talbot interferometer).

An example of interferograms with different shear distances are shown in Figs. 2(a) and 2(b), which were obtained by changing the grating separation distance D. If the position of the second grating is moved away in the x direction from the position of the first grating, the shear distance also increases in the vertical direction y. As a result, the precise control of two probe beams is possible, allowing for the implementation of a more rigorous differential interferometry in the laser-produced plasma diagnostics, compared with other interferometers.

The sensitivity of interferometric measurement tools is adjustable by changing the fringe width. Hence, it is essential to adjust the fringe width to attain an optimal signal-to-noise ratio for plasma density measurement. In practical experiments, the plasma density under diagnosis varies, often requiring dynamic adjustment of the fringe width. However, the fringe width in conventional interferometers is often correlated with other parameters, for example, coherence length for a Mach-Zehnder interferometer or plasma image location for a Nomarski interferometer, leading to difficulties for such adjustments. On the contrary, the fringe width in the proposed double-grating interferometer can be changed by rotation of the first grating G1 while keeping the plasma image positions of the probe beams constant.

Optics EXPRESS

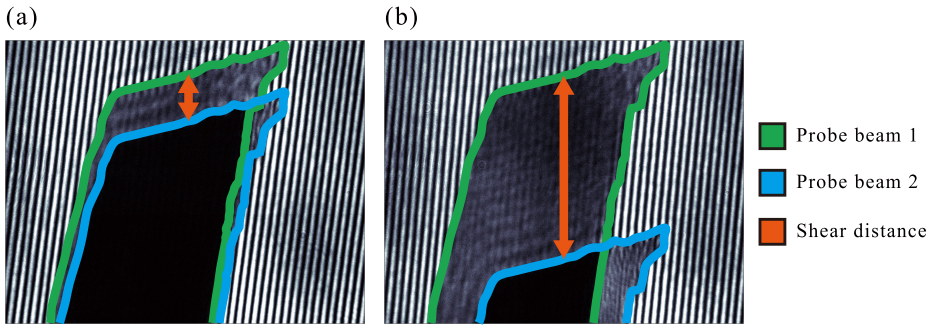

Fig. 2. (a) and (b): Interferograms with different shear distances when a wire tip is placed in the object plane. D values for (a) and (b) are 8 and 33 mm, respectively, in this case. Since the shear direction is fixed in the vertical direction, only the probe beam 2 image can move downward in the screen.

4. Plasma diagnostics with the new differential interferometer

4.1. Experimental setup

For performance test of the proposed double-grating differential interferometer, it was employed for diagnostics of the laser-produced plasma in our laboratory at GIST (Gwangju Institute of Science and Technology), where we have a 1 TW Ti:sapphire laser system [19] with a repetition rate of 10 Hz. As shown in Fig. 3, this laser system can deliver laser pulses with a pulse duration of 35 fs full width at half maximum (FWHM), a central wavelength of 800 nm and an FWHM bandwidth of 41.6 nm. In this experiment, the laser beam with an energy of 39 mJ and a diameter of 17 mm was divided into two beams by a 10:90 (R:T) beam splitter. The transmitted main laser pulse was focused in the nitrogen gas jet with a 100 μm diameter nozzle by using the off-axis parabolic mirror with a short focal length of 101.6 mm. In this case, the focused laser intensity is high enough, leading to a laser-produced plasma. The reflected low-intensity probe pulse passed through the plasma in the gas jet transversely and directed to the double-grating differential interferometer. The probe beam pulse was time-delayed by the delay line and its size was reduced by a telescope with two lenses (f = 150 mm, 65 mm). Then the probe beam was expanded by two telescopes. Magnifications of the two telescopes were 4 (f = 50 mm, 200 mm) and 3.75 (f = 40 mm, 150 mm), respectively. The second image formed after the two telescopes was imaged onto the CCD camera (GS3-U3-28S4M-C, FLIR) by using a bi-convex lens (f = 125 mm). In the double-grating differential interferometer for laser-produced plasma diagnostics, two identical 30 lp/mm Ronchi gratings were used. The first grating was positioned at the plasma image plane after the second telescope, and the second grating was placed after the first grating with the variable grating distance D for optimization of the shear distance s. An iris diaphragm was placed at the focal plane of the imaging lens to filter unnecessary high diffraction orders. An 800 nm bandpass filter ($\Delta\lambda$ = 4 nm) was inserted between the two magnifying telescopes to prevent any chromatic effects caused by diffraction from the gratings.

4.2. Experimental results

We performed experiments for plasma density diagnostics using the new double-grating-based differential interferometer. In experiments, the main laser beam of 35 mJ/pulse was focused at a distance of 150 μm above the nitrogen gas jet with a backing pressure of 4.2 bar and the focused laser intensity was high enough to produce a plasma. The laser-produced plasma was diagnosed by the new double-grating interferometer with a short grating distance and the results were compared with those obtained using the conventional method with a sufficient grating distance

Optics EXPRESS

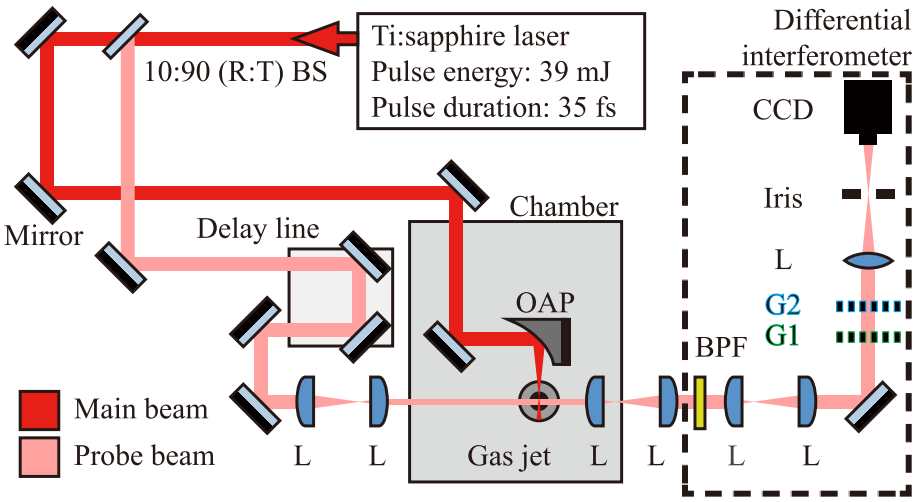

Fig. 3. Schematic diagram of the experimental setup. In the figure, the initial laser pulse with an energy of 39 mJ is divided by a beam splitter and the main laser pulse with 90 % energy is focused in the gas jet for laser-produced plasma generation, while the other low-intensity probe pulse passes through the laser-produced plasma transversely towards the double-grating differential interferometer. BS: beam splitter, OAP: off-axis parabolic mirror, BPF: bandpass filter, L: lens, G1, G2: gratings.

that can separate the second plasma image. A typical example of the measured interferograms by two methods is shown in Figs. 4(a) and 4(b). The 1-D wavelet transform was used for extraction of the fringe shifts from the interferograms [20]. To isolate fringe shifts induced only by the plasma from those caused by the gas jet, a reference fringe shift without the plasma was subtracted from the signal fringe shifts with the plasma and the results are shown in Figs. 4(c) and 4(d). Since the differential interferometer measures the phase shift gradient (not phase shift itself), the fringe lines shift in opposite directions in the upper and lower region of the plasma as shown in Fig. 4(a), while they shift in only one direction in the conventional method (Fig. 4(b)). Due to the tightly-focused main laser pulse, the edge of the laser-produced plasma, as indicated by the fringe shifts, can be clearly seen in the images. Before applying the Abel inversion for calculation of the plasma density, the shear distance and the actual pixel size were calibrated by placing a resolution target in the object plane where the real plasma was located. All interferograms and density measurements were taken 3 ps after the main laser pulse passed through the focal point from left to right (in $+z$ direction).

When the main Ti:sapphire laser pulse of 35 mJ is focused in the nitrogen gas jet, the estimated peak intensity of the laser pulse at the focal spot is about 2.2×10^{18} W/cm^2 based on the measured focal spot size, which is high enough to ionize nitrogen atoms up to the fifth electron. Furthermore, if the laser peak power P_L is above the relativistic self-focusing critical power $P_{cr} = 17.4 \times (n_{cr}/n_e)$ GW [21], the laser pulse can be further focused by the self-focusing effect. Here, n_{cr} is the plasma critical density given by $n_{cr} \approx 1.74 \times 10^{21}$cm^{-3} for 800 nm wavelength and n_e is the plasma density. In this way, the TW-class laser pulse can reach an intensity over 1×10^{19} W/cm^2 for further ionization of nitrogen [22]. The estimated laser peak power to critical power ratio P_L/P_{cr} in our case is expected to be about ~ 1.5 based on the measured peak plasma density. Therefore, the peak laser intensity can be enhanced by the relativistic self-focusing in the nitrogen plasma. As a result, a rather long plasma channel and a sharp plasma density gradient can be generated in the gas get.

Optics EXPRESS

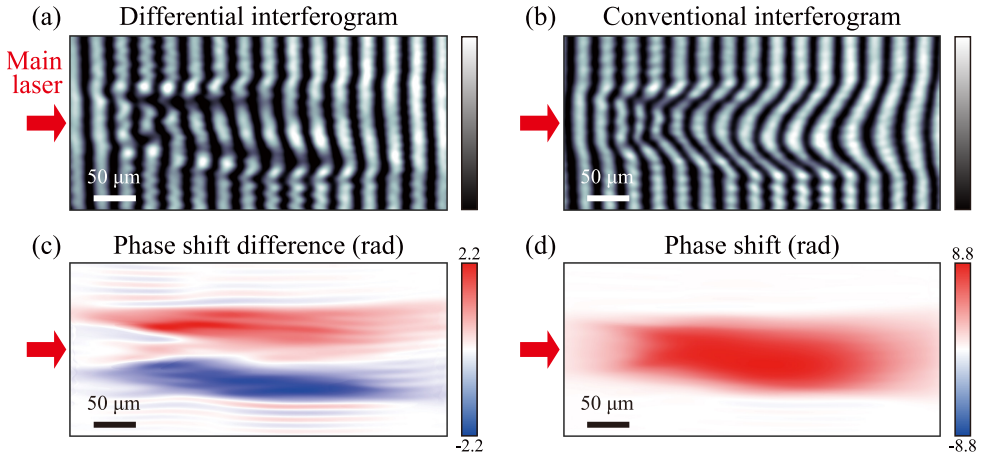

Fig. 4. Typical interferograms from (a) the differential interferometry and (b) the conventional interferometry. Retrieved phase information from (c) the differential interferometry and (d) the conventional interferometry. The red arrows indicate the direction of the main laser beam propagation. The images are taken 3 ps after plasma generation by focusing the 1 TW laser pulse in the 100 μm diameter gas jet of 4.2 bar backing pressure.

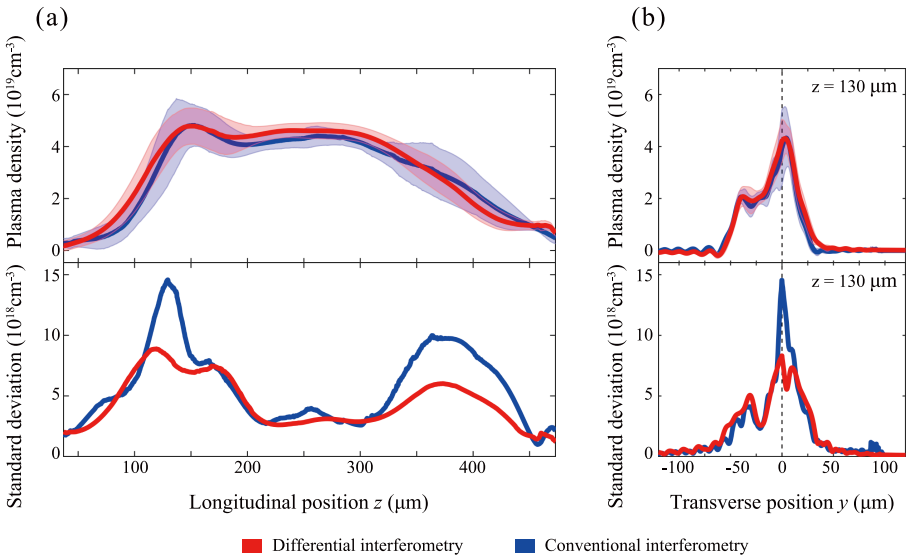

Fig. 5. Comparison results: (a) 25-shot averaged on-axis plasma densities and their standard deviations, and (b) 25-shot averaged radial plasma densities and their standard deviations at z = 130 μm, using the new differential interferometer and the conventional interferometer, respectively. The shaded areas in the upper figures represent standard deviations.

The plasma density information of laser-produced plasma channel in two different methods was obtained by applying the Abel inversion to the measured phase maps and the results were compared. The top of Fig. 5(a) shows the 25-shot averaged longitudinal plasma density profiles and the top of Fig. 5(b) shows the radial plasma density profiles at z = 130 μm, where the calibrated shear distance (~ 5 μm) is much smaller than the radial plasma size (~ 100 μm), validating the approximation in Eq. (1). The shaded area represents the standard deviations

Optics EXPRESS

of the measured plasma densities from 25 shots. Both density profiles from the differential and conventional methods give similar density profiles because the noises are suppressed by averaging over 25 shots. However, it should be noted that there are significant differences in the standard deviations of plasma densities between the two methods, as shown in the bottom figures of Figs. 5(a) and 5(b). The comparison results clearly indicate that the differential interferometery has much smaller uncertainties in plasma density measurements especially in the high spatial gradient region ($z = 130$ μm and $z = 360$ μm). As mentioned earlier, the discrepancy in standard deviations tends to be amplified, particularly at the center of the plasma while they have similar values in the outer regions as shown in Fig. 5(b). This fact implies that the new double-grating-based differential interferometer can provide a more reliable plasma density diagnostic result compared with other conventional interferometers.

5. Conclusions

In conclusion, a novel scheme of a double-grating interferometer was successfully developed for implementation of the differential interferometry, which is very useful for diagnostics of laser-produced plasmas. With this interferometer, the shear distance, shear direction, and fringe width can be adjusted completely independently while keeping the one plasma image position fixed. As a result, this interferometer can provide more fine manipulation of the two probe beams unlike any other known interferometers. In order to demonstrate the validity of the developed differential interferometer, a 1 TW laser system was used to generate a laser-produced plasma and it was proved that the developed double-grating-based differential interferometer can provide much more reliable density information especially in the high spatial gradient plasma. This method can be used for diverse applications, for example, in diagnostics of a high density and high gradient plasma for laser pulse compression [23] experiments in our laboratory.

Funding. National Research Foundation of Korea (2022R1A2C3013359, RS-2022-00154676, RS-2023-00218180).

Disclosures. The authors declare no conflicts of interest.

Data availability. Data underlying the results presented in this paper are not publicly available at this time but may be obtained from the authors upon reasonable request.

References

1. Z. H. He, B. Hou, J. A. Nees, *et al.*, "High repetition-rate wakefield electron source generated by few-millijoule, 30 fs laser pulses on a density downramp," New J. Phys. **15**(5), 053016 (2013).
2. F. Salehi, A. J. Goers, G. A. Hine, *et al.*, "Mev electron acceleration at 1 khz with < 10 mj laser pulses," Opt. Lett. **42**(2), 215–218 (2017).
3. L. Rovige, J. Huijts, I. Andriyash, *et al.*, "Demonstration of stable long-term operation of a kilohertz laser-plasma accelerator," Phys. Rev. Accel. Beams **23**(9), 093401 (2020).
4. Z. H. He, A. G. R. Thomas, B. Beaurepaire, *et al.*, "Electron diffraction using ultrafast electron bunches from a laser-wakefield accelerator at kHz repetition rate," Appl. Phys. Lett. **102**(6), 064104 (2013).
5. J. Faure, B. van der Geer, B. Beaurepaire, *et al.*, "Concept of a laser-plasma-based electron source for sub-10-fs electron diffraction," Phys. Rev. Accel. Beams **19**(2), 021302 (2016).
6. J. Bourhis, P. Montay-Gruel, P. Gonçalves Jorge, *et al.*, "Clinical translation of flash radiotherapy: Why and how?" Radiother. Oncol. **139**, 11–17 (2019).
7. M. Cavallone, L. Rovige, J. Huijts, *et al.*, "Dosimetric characterisation and application to radiation biology of a khz laser-driven electron beam," Appl. Phys. B **127**(4), 57 (2021).
8. R. Álvarez, A. Rodero, and M. Quintero, "An abel inversion method for radially resolved measurements in the axial injection torch," Spectrochim. Acta, Part B **57**(11), 1665–1680 (2002).
9. U. Kogelschatz, "Application of a simple differential interferometer to high current arc discharges," Appl. Opt. **13**(8), 1749–1752 (1974).
10. O. Kafri, "Noncoherent method for mapping phase objects," Opt. Lett. **5**(12), 555–557 (1980).
11. D. E. Silva, "Talbot interferometer for radial and lateral derivatives," Appl. Opt. **11**(11), 2613–2624 (1972).
12. R. E. Walkup, J. M. Jasinski, and R. W. Dreyfus, "Studies of excimer laser ablation of solids using a Michelson interferometer," Appl. Phys. Lett. **48**(24), 1690–1692 (1986).
13. A. J. Gonsalves, T. P. Rowlands-Rees, B. H. P. Broks, *et al.*, "Transverse interferometry of a hydrogen-filled capillary discharge waveguide," Phys. Rev. Lett. **98**(2), 025002 (2007).

Optics EXPRESS

14. J. Kim, V. L. J. Phung, K. Roh, *et al.*, "Development of a density-tapered capillary gas cell for laser wakefield acceleration," Rev. Sci. Instrum. **92**(2), 023511 (2021).
15. R. Benattar, C. Popovics, and R. Sigel, "Polarized light interferometer for laser fusion studies," Rev. Sci. Instrum. **50**(12), 1583–1586 (1979).
16. P. Tomassini and A. Giulietti, "A generalization of abel inversion to non-axisymmetric density distribution," Opt. Commun. **199**(1-4), 143–148 (2001).
17. V. Ronchi, "Forty years of history of a grating interferometer," Appl. Opt. **3**(4), 437–451 (1964).
18. Y. Song, Y. Y. Chen, A. He, *et al.*, "Theoretical analysis for moiré deflectometry from diffraction theory," J. Opt. Soc. Am. A **26**(4), 882–889 (2009).
19. V. L. J. Phung, K. Kang, S. Jeon, *et al.*, "Development of a 1 tw/35 fs ti:sapphire laser amplifier and generation of intense thz waves using two-color laser filamentation," Photonics **8**(8), 316 (2021).
20. J. Zhong and J. Weng, "Phase retrieval of optical fringe patterns from the ridge of a wavelet transform," Opt. Lett. **30**(19), 2560–2562 (2005).
21. G. Z. Sun, E. Ott, Y. C. Lee, *et al.*, "Self-focusing of short intense pulses in plasmas," Phys. Fluids **30**(2), 526–532 (1987).
22. S. Augst, D. D. Meyerhofer, D. Strickland, *et al.*, "Laser ionization of noble gases by coulomb-barrier suppression," J. Opt. Soc. Am. B **8**(4), 858–867 (1991).
23. M. S. Hur, B. Ersfeld, H. Lee, *et al.*, "Laser pulse compression by a density gradient plasma for exawatt to zettawatt lasers," Nat. Photonics **17**(12), 1074–1079 (2023).